# 2

# Corrosion Resistance of Directionally Solidified Casting Zinc-Aluminum Matrix

Alicia Esther Ares[1,2,3], Liliana Mabel Gassa[1,4]
and Claudia Marcela Mendez[3]
[1] *Researcher of CIC, CONICET,*
[2]*Materials, Modeling and Metrology Program,*
*Faculty of Sciences, National University of Misiones, Posadas,*
[3]*Materials Laboratory, Faculty of Sciences, National University of Misiones, Posadas,*
[4]*INIFTA, National University of La Plata, Faculty of Exact Sciences, La Plata,*
*Argentina*

## 1. Introduction

Generally solidification leads to two types of grain morphologies: columnar and equiaxed. The origin of each one has been the subject of numerous theoretical and experimental researches in the field of metallurgy for many years. Columnar grains often grow from near the mold surface, where the thermal gradients are high, and the growth is preferentially oriented in a direction close to the heat flux. When the gradients are reduced near the center of the casting, equiaxed grains grow in all space directions leading to a material with more isotropic macroscopic mechanical properties and a more homogeneous composition field than with columnar structure. Depending on the application, one type of grain is preferred and thus favoured, e.g. equiaxed grains in car engines and columnar grains in turbine blades as reported by Reinhart et al, 2005 and McFadden et al., 2009.

Since the grain structure influences the properties of a casting, a great deal of effort has been devoted in the last decades to understand the mechanism behind the development of the macrostructure during solidification. Thus, equiaxed grains can nucleate and grow ahead of the columnar front causing an abrupt columnar to equiaxed transition (CET) whose prediction is of great interest for the evaluation and design of the mechanical properties of solidified products. As a consequence, it is critical for industrial applications to understand the physical mechanisms which control this transition during solidification (Spittle, 2006).

In order to realize the control of the columnar and equiaxed growth, it is necessary to understand the columnar to equiaxed transition (CET) mechanism during solidification, and make clear the CET transition condition. Fundamentally, it is necessary to have knowledge of the competition between nucleation and growth during solidification. Qualitatively, the CET occurs more easily when an alloy has a high solute concentration, low pouring temperature (for casting), low temperature gradient, high nucleation density in the melt and vigorous melt convection.

However, a quantitative understanding of the CET requires a thorough comprehension of all physical mechanisms involved.

In 1984, Hunt first developed an analytical model to describe steady-state columnar and equiaxed growth, and to qualitatively reveal the effects of alloy composition, nucleation density and cooling rate on the CET. On the other hand, he used a very simple empirical relationship to describe the variation of the undercooling with alloy composite and solidification rate. Cockcroft et al. (1994) used a more recent growth theory for the columnar and equiaxed growth but without considering high velocity non-equilibrium effects under rapid solidification. Recently, based on Hunt's CET model, Gäumann et al. (1997, 2001) developed a more comprehensive model by combining KGT model (Kurtz et. al., 1986) for directional solidification with LKT model (Lipton et. al., 1987) for the undercooling melt growth, with high velocity non-equilibrium effects to be taken into account. Gäumann et al. (2001) succeeded in applying their model to epitaxial laser metal forming of single crystal.

In previous research, the authors of this work carried out experiments in which the conditions of columnar to equiaxed transition (CET) in directional solidification of dendritic alloys were determined The alloy systems in this work include Pb–Sn (Ares & Schvezov, 2000), Al–Cu (Ares et. al., 2011), Al–Mg (Ares et. al., 2003), Al–Zn and Zn-Al alloys (Ares & Schvezov, 2007). These experiments permit to determine that the transition occurs gradually in a zone when the gradient in the liquid ahead of the columnar dendrites reaches critical and minimum values, being negative in most of the cases. The temperature gradients in the melt ahead of the columnar dendrites at the transition are in the range of -0.80 to 1.0 $^{o}$C/cm for Pb–Sn, -11.41 to 2.80 $^{o}$C/cm for Al–Cu, -4.20 to 0.67 $^{o}$C/cm for Al–Si, -1.67 to 0.91 $^{o}$C/cm for Al–Mg, -11.38 to 0.91 $^{o}$C/cm for Al–Zn. Two interphases are defined; assumed to be macroscopically flat, which are the liquidus and solidus interphases. After the transition, the speed of the liquidus front accelerates much faster than the speed of the solidus front; with values of 0.004 to 0.01, 0.02 to 0.48, 0.12 to 0.89, 0.10 to 0.18 and 0.09 to 0.18 cm/s, respectively. Also, the average supercooling of 0.63 to 2.75 1C for Pb–Sn, 0.59 to 1.15 1C for Al–Cu, 0.67 to 1.25 1C for Al–Si, 0.69 to 1.15 1C for Al–Mg, 0.85 to 1.40 1C for the Al–Zn and was measured, which provides the driving force to surmount the energy barrier required to create a viable solid–liquid interface (Ares et al., 2005). A semi-empirical model to predict the columnar to equiaxed transition is developed based on experimental results obtained from measurements during solidification of lead–tin alloys directly upwards (Ares et al., 2002). The measurements include the solidification velocities of the liquidus and solidus fronts, and the temperature gradients along the sample in the three regions of liquid, mushy and solid. The experimental data was coupled with a numerical model for heat transfer. With the model, the predicted positions of the transition are in agreement with the experimental observations which show that the transition occurs when the temperature gradient reaches values below 1$^{o}$C/cm and the velocity of the liquidus front increases to values around 0.01cm/s.

In addition, the thermal parameters, type of structure, grain size and dendritic spacing with the corrosion resistance of Zn-4wt%Al, Zn-16wt%Al and Zn-27wt%Al alloys were correlated (Ares et al., 2008). The polarization curves showed that the columnar structure is the most susceptible structure to corrosion, in the case of the alloy with only 4wt%of Al. The rest of the structures presented currents of peaks in the same order which were independent to the concentration of Al composition presenting in the alloy.

The biggest susceptibility to corrosion of the alloys with columnar structure can be observed by analyzing the values of Rct (charge transfer resistance) obtained using the electrochemical impedance spectroscopy (EIS) technique. In Zn-4wt%Al and Zn-27wt%Al, the corrosion susceptibility depends on the structure of the alloy. The alloy with 16wt%Al is less resistant to corrosion and their susceptibility to corrosion is independent of the structure. The alloy with 27wt%Al and the CET structure is the alloy which has the most corrosion resistance. When the critical temperature gradient becomes more negative, the Rct values increase. In the case of the correlation of Rct values and the structural parameters such as the grain sizes and secondary dendritic spacing, Rct values increase when the grain size and secondary dendritic spacing increase. But this does not happen for ZA16 alloy.

Composite materials obtained by solidification of alloys have made remarkable progress in their development and applications in automotive and aerospace industries in recent decades. Among them the most current applications are the zinc and aluminum base composite materials (Long et al., 1991; Rohatgi, 1991). It is well-known that the corrosion behavior of MMCs is based on many factors such as the composition of the alloy used, the type of reinforcement particles used, the reinforcement particle sizes and their distribution in the matrix, the technique used for the manufacture, and the nature of the interface between the matrix and reinforcement. A very slight change in any of these factors can seriously affect the corrosion behavior of the material.

In short, there is little research related to the study of mechanical and electrochemical properties of Zn-Al alloys as well as Zn-Al alloys MMCs containing SiC and $Al_2O_3$ particulations with different grain structures in the matrix. Also there is lack of fundamental study on the performance of Zn-Al alloys and their MMCs in corrosive environments when both solidification microstructure and type of particle distribution are in consideration. In the present research, Zn-Al-SiC and Zn-Al-$Al_2O_3$ composites are prepared and solidified by vertical directional solidification method. By means of voltammograms and electrochemical impedance spectroscopy, the corrosion resistances of Zn-Al matrix composite materials with different types of particles are obtained and analyzed and the results are compared.

## 2. Materials and methods

### 2.1 Alloys and metal matrix composites preparation

Zinc-Aluminum (ZA) alloys of different compositions were prepared from zinc (99.98 wt pct), aluminum (99.94 wt pct), and composites were prepared by adding SiC and $Al_2O_3$ particles to the alloys. The compositions of the alloys and composites prepared and directionally solidified are: Zn-27wt%Al, Zn-50wt%Al, Zn-27wt%Al + 8vol%SiC, Zn-27wt%Al + 15vol% SiC, Zn-50wt%Al + 8vol%SiC, Zn-50wt%Al + 15vol%SiC, Zn-27wt%Al + 8vol%$Al_2O_3$, Zn-27wt%Al + 15vol%$Al_2O_3$.

The chemical compositions of the commercially pure metals used to prepare the alloys are presented in Table 1. The molds were made from a 23 mm i.d. and 25 mm e.d. PYREX (Corning Glass Works, Corning, NY) tube, with a flat bottom, a cylindrical uniform section and a height of 200 mm. The sample was a cylinder 22 mm in diameter and 100 mm in height.

| Chemical composition of Zn | |
|---|---|
| Element | Weight percent, wt% |
| Zn | 99.98 ± 0.2 |
| Fe | 0.010 ± 0.01 |
| Si | 0.006 ± 0.0001 |
| Pb | 0.004 ± 0.001 |
| Others | < 0.001 ± 0.0001 |
| Chemical composition of Al | |
| Element | Weight percent, wt% |
| Al | 99.94 ± 0.2 |
| Fe | 0.028 ± 0.0001 |
| Si | 0.033 ± 0.001 |
| Pb | 0.001 ± 0.0001 |
| Others | < 0.001 ± 0.0001 |

Table 1. Chemical composition of the Zn and Al used to prepare the alloys.

### 2.2 Directional solidification

The alloy samples were melted and solidified directionally upwards in an experimental set-up described elsewhere (Ares et. al., 2007). It was designed in such a way that the heat was extracted only through the bottom promoting upward directional solidification to obtain the columnar-to-equiaxed transition (CET), see Figure 1 (a).

In order to reveal the macrostructure, after solidification the samples were cut in the axial direction, polished, and etched using concentrated hydrochloric acid for 3 seconds at room temperature for the zinc-aluminum alloys, followed by rinsing and wiping off the resulting black deposit. The microstructures were etched with a mixture containing chromic acid (50 g $Cr_2O_3$; 4 g $Na_2SO_4$ in 100 ml of water) for 10 seconds at room temperature (Vander Voort, 2007). Typical longitudinal macrostructure of different areas of the sample are shown in Figure 1 (b) to (d).

The position of the transition was located by visual observation and optical microscopy. The distance from the chill zone of the sample was measured with a ruler. It is noted in Figure 1 that the CET is not sharp, showing an area where some equiaxed grains co-exist with columnar grains. As was reported before, the size of the transition area is in the order of up to 10 mm (Ares et al., 2007, 2010). The grain structure was inspected by visual observation under Arcano® optical microscopy.

### 2.3 Corrosion tests

For the electrochemical tests, samples of 20 mm in length of each zone and for each concentration were prepared as test electrodes (see Figure 1), polished with sandpaper (from SiC #80 until #1200) and washed with distilled water and dried by natural flow of air.

All the electrochemical tests were conducted in 3wt% NaCl solution at room temperature using an IM6d Zahner®-Elektrik potentiostat coupled to a frequency analyzer system.

A conventional three-compartment glass electrochemical cell with its compartments separated by ceramic diaphragms was used. The test electrodes consisted of sections of the ZA ingots (see Figure 1) were positioned at the glass corrosion cell kit (leaving a rectangular area in contact with the electrolyte). The potential of the test electrode was measured against a saturated calomel reference electrode (0.242 V vs NHE), provided with a Luggin capillary tip. The Pt sheet was used as a counter electrode.

Voltammograms were run between preset cathodic (open circuit potential ≈ -1.500 V) and anodic (Es,a = -0.700 V) switching potentials at potential sweep rates (v), at 0.002 $V.s^{-1}$. Impedance spectra were obtained in the frequency range of $10^{-3}$ Hz and $10^{5}$ Hz at open circuit potential.

For comparison purposes, experiments using pure metals and aluminum-based alloys with different structures were conducted under the same experimental conditions. All the corrosion tests experiments were triplicate and the average values and graphical outputs are reported.

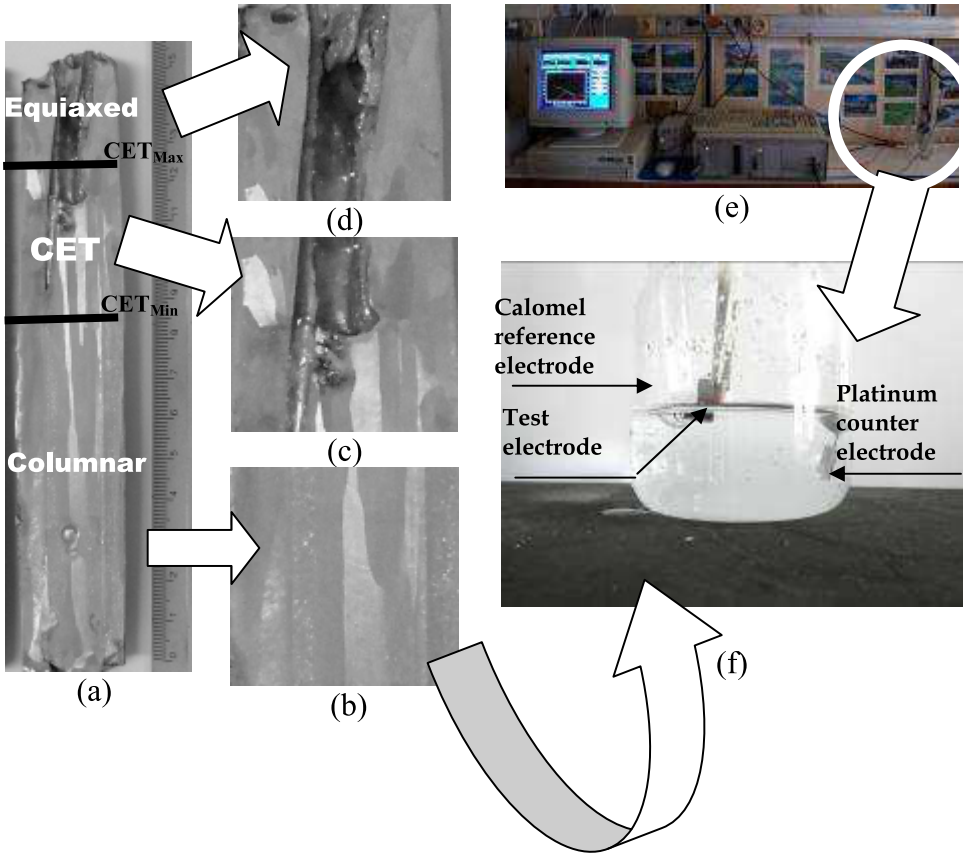


Fig. 1. Experimental device for electrochemical tests. (f) A glass corrosion cell kit with a platinum counter electrode and a sutured calomel reference electrode (SCE).

## 3. Results and discussion

### 3.1 Voltammetric data

During the anodic potential scanning, the voltammogram of equiaxed zinc shows that the current is practically zero until it reaches a potential of -1 V, where the current rises sharply, starting the active dissolution of metal (Figure 2 (a)). The negative potential scan shows a hysteresis loop, suggesting that this current increase was due to the start of a process of pitting, and two cathodic current peaks at about -1.2 V and - 1.3 V (called $C_1$ and $C_2$). These peaks could be associated with the reduction of $Zn(OH)_2$ and ZnO, respectively (Zhang, 1996). The composition of corrosion products formed on the zinc surface may be not uniformly distributed. The different compositions of the films formed can explain the difference in the outcomes reported in the literature.

The properties of corrosion products are a function of various material and environmental factors and thus vary essentially from situation to situation. For example, only one peak appears in the case of the columnar zinc (Figure 2 (b)). As the concentration of aluminum in the alloy increases, the definition of these reduction peaks is not clear, although the $C_2$ peak is dominant (Figure 2 (c)).

In the case of the alloys, the values of the anodic currents are similar for the same Al concentration, independently of the structure, and the most important difference is observed in the distribution of the cathodic current peaks, which indicates the different characteristics of the films formed during the anodic scan. These results can be attributed to the aggressive/depassivating action of $Cl^-$ anions (Augustynski, 1978). At present, the mechanism of film formation is still uncertain. For the case of CET structure, profiles are more complex, because the proportion of one or other structure (columnar or equiaxed) can vary from sample to sample (Figure 2 (d)). Also, as the concentration of Al increases, the voltammetric profile of the different structures tends towards the response of pure aluminum (Figure 2 (e)).

Analyzing the response of the composites (Zn-27wt%Al + 8vol%SiC, Zn-27wt%Al + 15vol%SiC (Figure 2(f)), Zn-50wt%Al + 8vol%SiC, Zn-50wt%Al + 15vol%SiC (Figure 4 (g)), Zn-27wt%Al + 8vol%$Al_2O_3$, Zn-27wt%Al + 15vol%$Al_2O_3$ (Figure 2 (h))), we observed that when the volume percent of SiC particles increase from 8% to 15% in ZA27 and ZA50 matrix, the rate of dissolution of the alloy increases. In the case of the addition of $Al_2O_3$ particles to ZA 27 matrix the rate of dissolution is approximately the same.

This different distribution of the peaks in the voltammograms gives rise to surface layers with different corrosion products, as shown in the micrographs of Figure 3, where samples with higher proportion of particles in the matrix show the formation of a thicker layer of corrosion products. Also, it is observed the formation of pitting on the electrode surface.

Three distinctive features in the potentiodynamic curves can be clearly observed (Figure 4): (i) the potential at which the anodic current during the forward anodic bias increases sharply form the passive current level (breakdown or critical pitting potential $E_p$); (ii) a hysteresis loop (difference between forward and reverse scans) and (iii) the potential at which the hysteresis loop is completed during reverse polarization scan after localized corrosion propagation (repassivation potential $E_r$). Stable pits form at potentials noble to $E_p$ and will grow at potentials noble to Er (Frankel, 1998). Also, for many years it has been recognized that Ep measurements are applicable to naturally occurring pit initiation on stainless alloys in chemical and marine environments (Wilde, 1972; Bilmes et al., 2005).

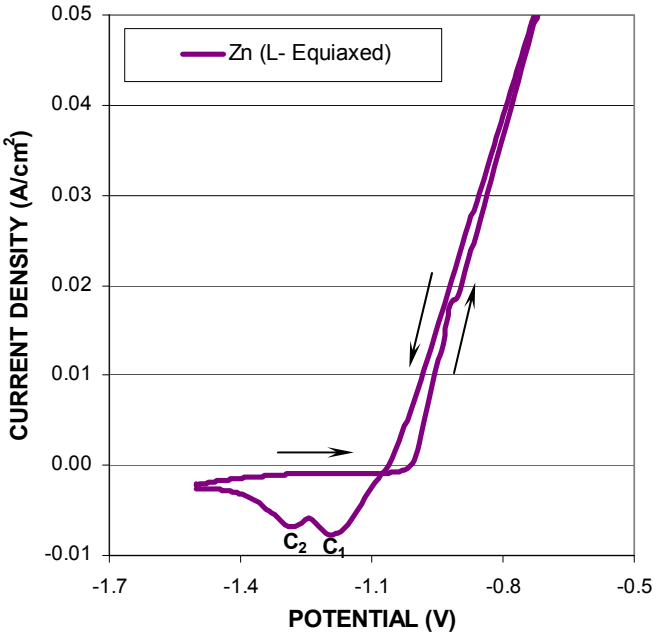
Zn (L- Equiaxed)
CURRENT DENSITY (A/cm2)
0.05
0.04
0.03
0.02
0.01
0.00
-0.01
C2
C1
-1.7
-1.4
-1.1
-0.8
-0.5
POTENTIAL (V)

(a)

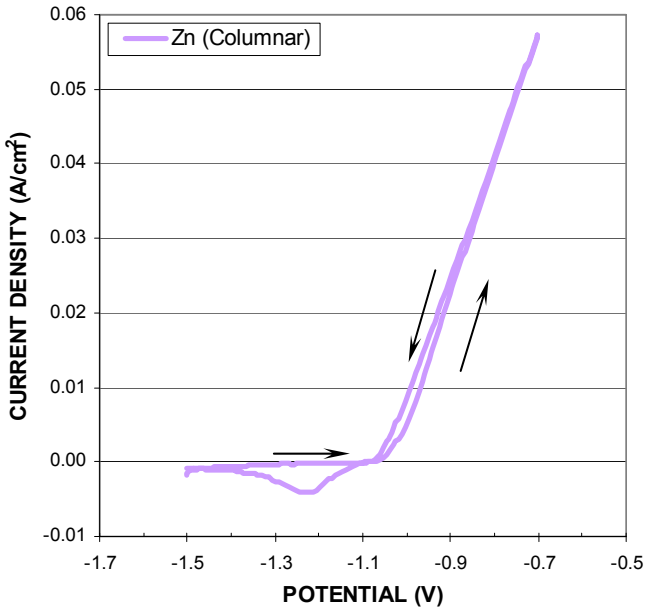
Zn (Columnar)
CURRENT DENSITY (A/cm2)
0.06
0.05
0.04
0.03
0.02
0.01
0.00
-0.01
-1.7
-1.5
-1.3
-1.1
-0.9
-0.7
-0.5
POTENTIAL (V)

(b)

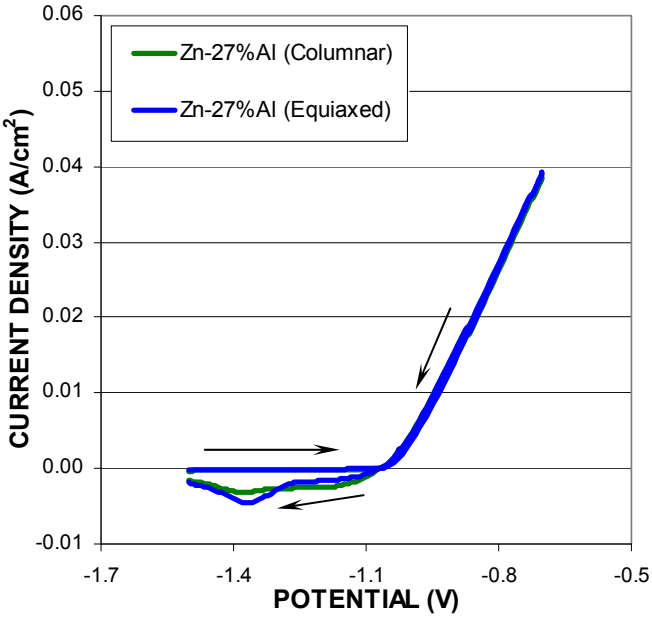
Zn-27%Al (Columnar)
Zn-27%Al (Equiaxed)
CURRENT DENSITY (A/cm2)
0.06
0.05
0.04
0.03
0.02
0.01
0.00
-0.01
-1.7
-1.4
-1.1
-0.8
-0.5
POTENTIAL (V)

(c)

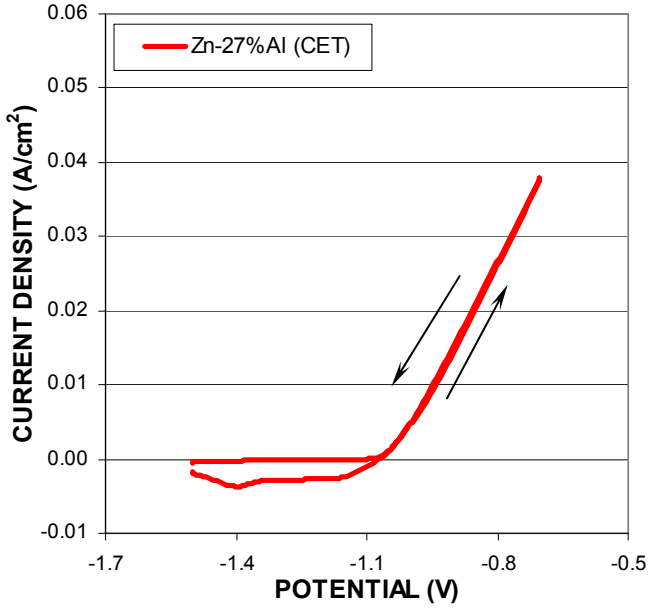
Zn-27%Al (CET)
CURRENT DENSITY (A/cm2)
0.06
0.05
0.04
0.03
0.02
0.01
0.00
-0.01
-1.7
-1.4
-1.1
-0.8
-0.5
POTENTIAL (V)

(d)

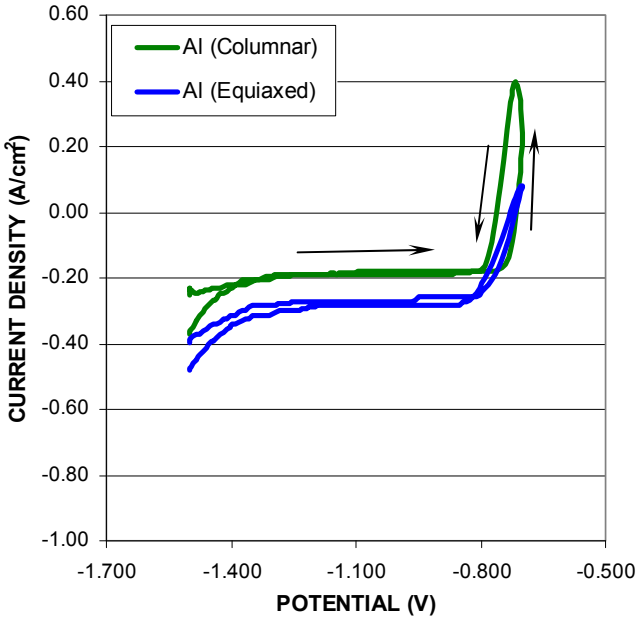
Al (Columnar)
Al (Equiaxed)
CURRENT DENSITY (A/cm2)
0.60
0.40
0.20
0.00
-0.20
-0.40
-0.60
-0.80
-1.00
-1.700
-1.400
-1.100
-0.800
-0.500
POTENTIAL (V)

(e)

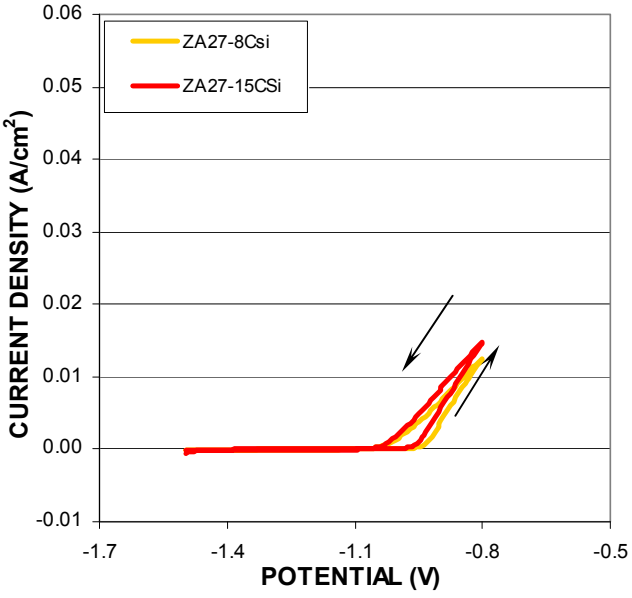
ZA27-8Csi
ZA27-15CSi
CURRENT DENSITY (A/cm2)
0.06
0.05
0.04
0.03
0.02
0.01
0.00
-0.01
-1.7
-1.4
-1.1
-0.8
-0.5
POTENTIAL (V)

(f)

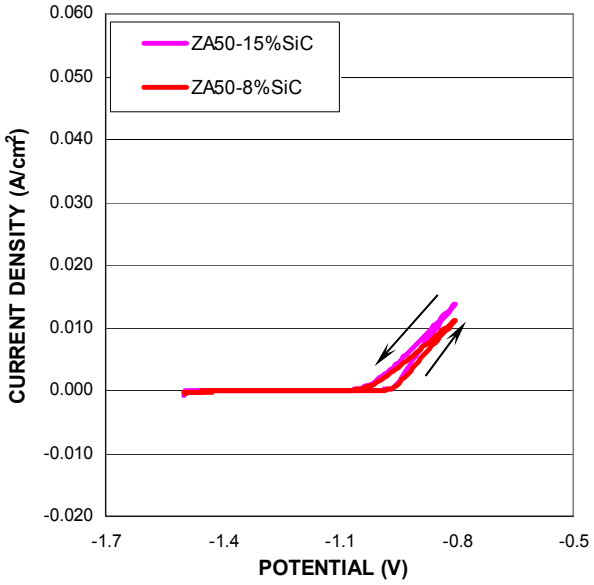
ZA50-15%SiC
ZA50-8%SiC
CURRENT DENSITY (A/cm2)
0.060
0.050
0.040
0.030
0.020
0.010
0.000
-0.010
-0.020
-1.7
-1.4
-1.1
-0.8
-0.5
POTENTIAL (V)

(g)

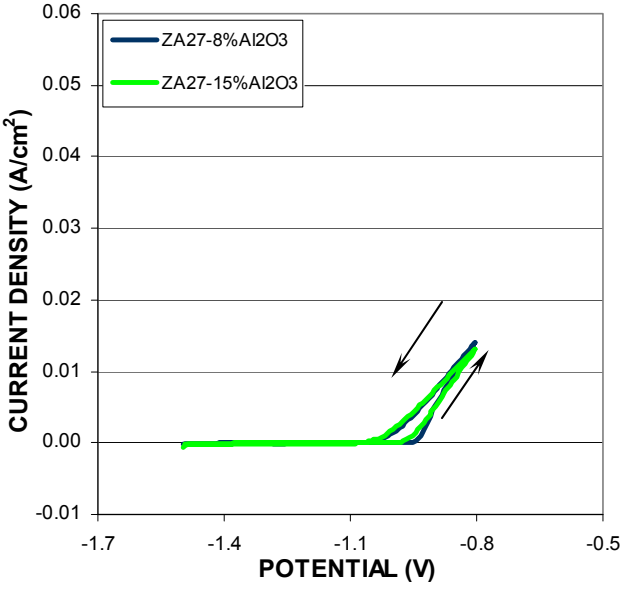
ZA27-8%Al2O3
ZA27-15%Al2O3
CURRENT DENSITY (A/cm2)
0.06
0.05
0.04
0.03
0.02
0.01
0.00
-0.01
-1.7
-1.4
-1.1
-0.8
-0.5
POTENTIAL (V)

(h)

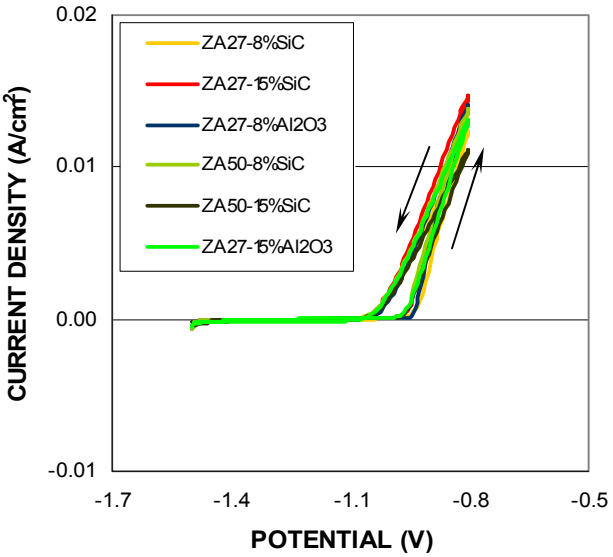


(i)

Fig. 2. Voltammograms of (a) pure Zinc with equiaxed structure, (b) pure Zinc with columnar structure (c) Zn-27wt%Al alloy with columnar and equiaxed structures, (d) Zn-27wt%Al alloy with CET structure, (e) pure Aluminum with columnar and equiaxed structure, (f) Zn-27wt%Al + 8vol%SiC, Zn-27wt%Al + 15vol%SiC, (g) Zn-50wt%Al + 8vol%SiC, Zn-50wt%Al + 15vol%SiC, (h) Zn-27wt%Al + 8vol%$Al_2O_3$, Zn-27wt%Al + 15vol%$Al_2O_3$ and (i) All types of composites.

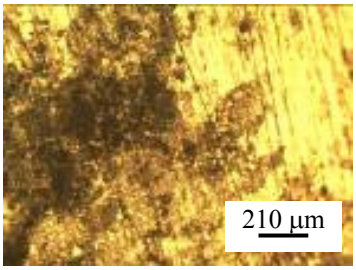


(a) Zn-Columnar

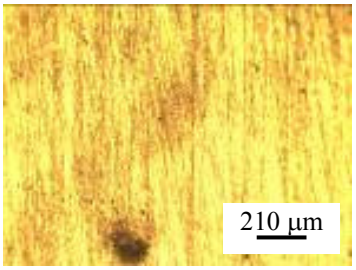


(b) Zn – Equiaxed

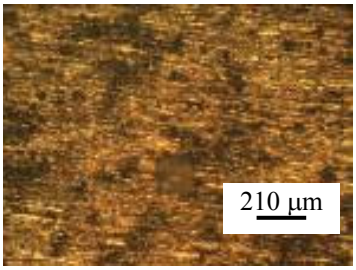


(c) Al-Columnar

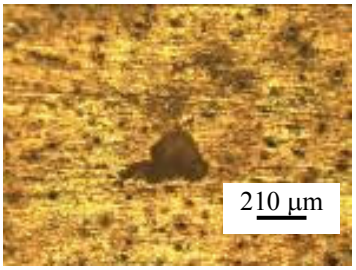


(d) Al – Equiaxed

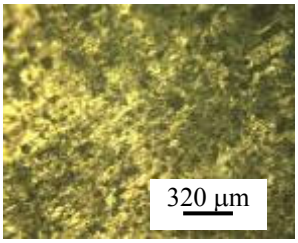


(e) Zn-27%Al-Columnar

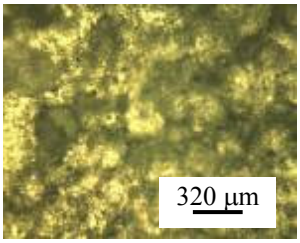


(f) Zn-27%Al – Equiaxed

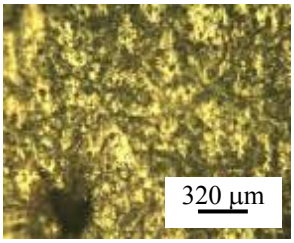


(g) Zn-27%Al – CET

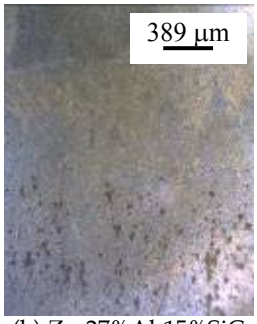


(h) Zn-27%Al-15%SiC

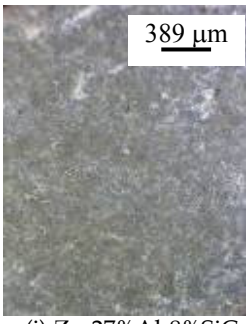


(i) Zn-27%Al-8%SiC

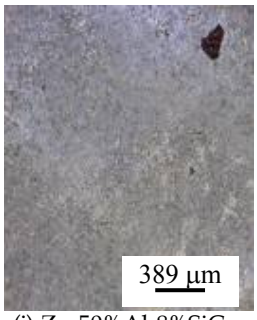


(j) Zn-50%Al-8%SiC

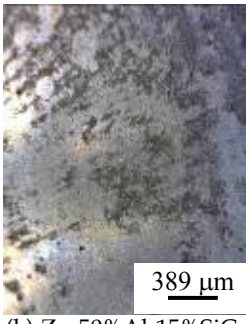


(k) Zn-50%Al-15%SiC


(l) Zn-27%Al-15%$Al_2O_3$

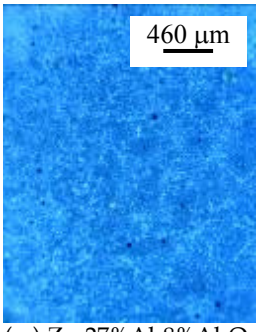


(m) Zn-27%Al-8%$Al_2O_3$

Fig. 3. Micrographs of different alloy samples and structures.

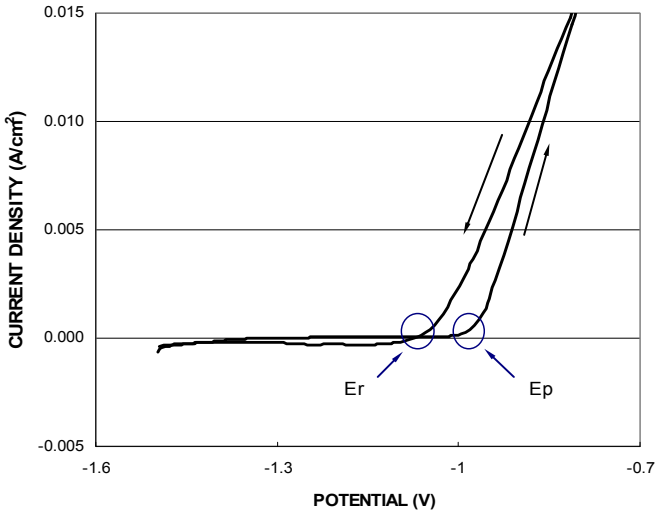


Fig. 4. Representative curve.

In all cases, the E / I response of the alloys shows the typical hysteresis indicates the phenomenon of pitting and found that the more susceptible are the composites than the alloys. The most susceptible are those containing neither SiC nor $Al_2O_3$ in the matrix, see Table 2 and Figure 5.

| Alloy / Composite | Ep (V) | Er (V) | ΔEp-r (mV) | Ecorr (V) | ΔEr-corr (mV) |
|---|---|---|---|---|---|
| ZA50-15vol%SiC | -1.002 | -1.093 | 91 | -1.271 | 178 |
| ZA50-8vol%SiC | -0.988 | -1.082 | 94 | -1.302 | 220 |
| ZA27-8vol%$Al_2O_3$ | -0.974 | -1.086 | 112 | -1.297 | 211 |
| ZA27-15vol%$Al_2O_3$ | -0.974 | -1.079 | 105 | -1.298 | 219 |
| ZA27-15vol%SiC | -1.002 | -1.086 | 84 | -1.312 | 226 |
| ZA27-8vol%SiC | -0.981 | -1.107 | 126 | -1.245 | 138 |
| ZA27 CET | -1.02 | -1.06 | 30 | -1.102 | 42 |
| ZA27 Col | -1.028 | -1.052 | 24 | -1.071 | 19 |
| ZA27 Eq | -1.038 | -1.068 | 40 | -1.068 | 0 |

Table 2. The susceptibility to corrosion, ΔE, was measured as the difference between the potential of pitting, Ep, and the repassivation potential, Er.

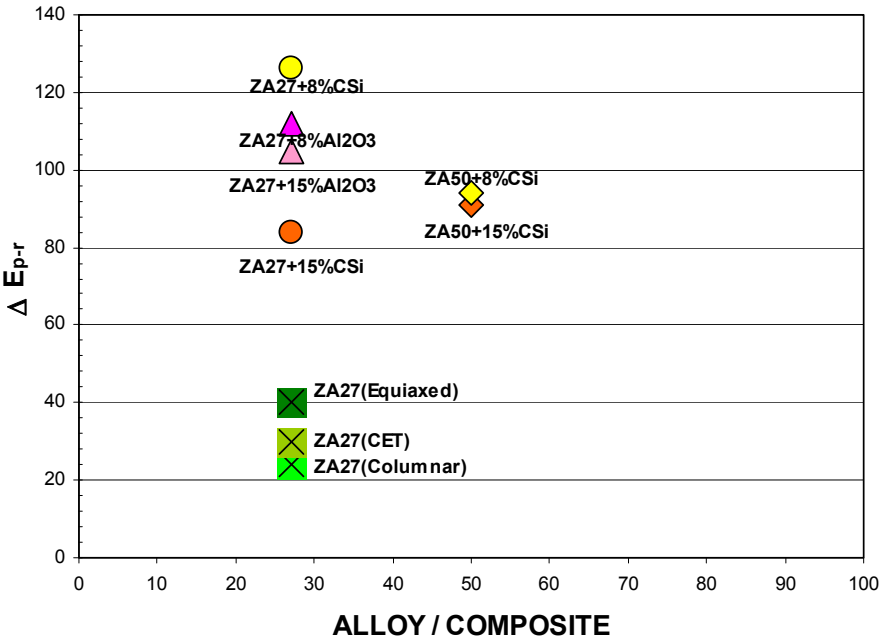


Fig. 5. $\Delta E_{p-r}$ as a function of concentration and alloy structure.

The susceptibility to corrosion was measured as the difference between the potential of pitting, Ep, and the repassivation potential, Er, as Δ Ep-r and the difference between the repassivation potential and the corrosion potential of each sample through Table 2 it is possible to observe that the values of repassivation potential for materials without particles in the matrix are near the corrosion potential, but not in the case of the the other samples.

### 3.2 Electrochemical impedance spectroscopy data

Impedance spectra are strongly dependent on the composition and structures of the alloys and composites. Figure 6 shows the experimental Nyquist diagrams for all the alloys and composites used. All the diagrams show one capacitive time constant at high frequencies and a non-well defined time constant at low frequencies, probably associated with diffusion processes also reported in the literature (Deslouis et al., 1984; Trabanelli at al., 1975). It can be seen that as the concentration of aluminum in the alloy increases, the second time constant approximates the response associated with a diffusion process in finite thickness, due to the formation of a more compact oxide.

In some cases, the shape of the Nyquist diagrams for CET structure in alloys resembles that of those with equiaxed structure and in others those with columnar structure, depending on the relative amount of each phase in the CET structure, which in turn depends on the region where the specimen was obtained.

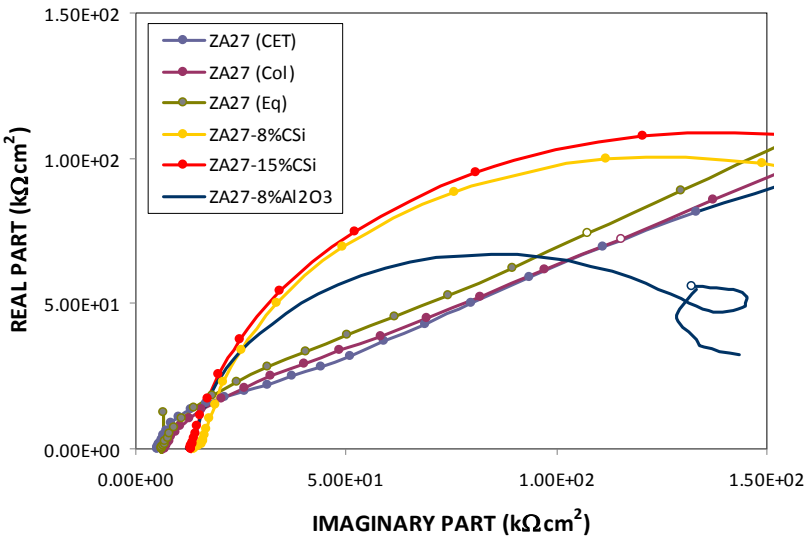


Fig. 6. (a) Nyquist Diagram for different samples.

The whole set of experimental impedance spectra can be discussed according to the following total transfer function.

$$Z_t(jw) = R_\Omega + Z \tag{1}$$

with:

$$\frac{1}{Z} = \frac{1}{R_{ct} + Z_W} + j_W.C \tag{2}$$

where $R_\Omega$ is the ohmic solution resistance, $\omega = 2\pi f$; $C_{dl}$ the capacitance of the electric double layer, $R_{ct}$ the charge transfer resistance and $Z_W$ the diffusion contributions in impedance spectra.

$Z_W = R_{DO}\,(jS)^{-05}$ for semi-infinite diffusion contribution and $Z_W = R_{DO}\,(jS)^{-05}\coth(jS)^{-05}$ is related to diffusion through a film of thickness d, formed on the electrode, where $R_{DO}$ is the diffusion resistance and the parameter $S = d2\omega/D$, where d and D are the diffusion thickness and diffusion coefficient related to the transport process (Fedrizzi et al., 1992).

The good agreement between experimental and simulated data according to the transfer function given in the analysis of Eqs. 1 and 2 using non-linear least square fit routines is shown in Figure 8 (a) at high frequencies. At low frequencies (less than 10-1 Hz) is not achieved a good fit with this model, since the impedance measurement does not give us enough information to define a new input capacitance, this occurs for samples ZA27-8% SiC, ZA50-8% SiC and ZA27-Al2O3. This process can represent by an equivalent circuit in Figure 8 (a).

For ZA27samples and those containing 15%SiC at high frequencies seems to be defined one second capacitive loop corresponding to corrosion processes controlled by precipitation and dissolution of ions Zn, see Figure 7 (b, c and d). The equivalent circuit corresponds to that showed in Figure 8 (b).

The values of $C_{dl}$, $C_1$ and $R_{ct}$ determined from the optimum fit procedure are presented in Table 3.

The analysis of the impedance parameters associated with the time constant at low frequencies is difficult because in some cases the loop it is not complete. However, it was possible to calculate from by fitting an approximate value of diffusion coefficient D ≈ $10^{-10}$ – $10^{-12}$ $cm^2/s$.

High values of capacity confirm the formation of porous corrosion products, as can be seen in Figure 9. These high values of capacity may also be correlated with an increase in the area.

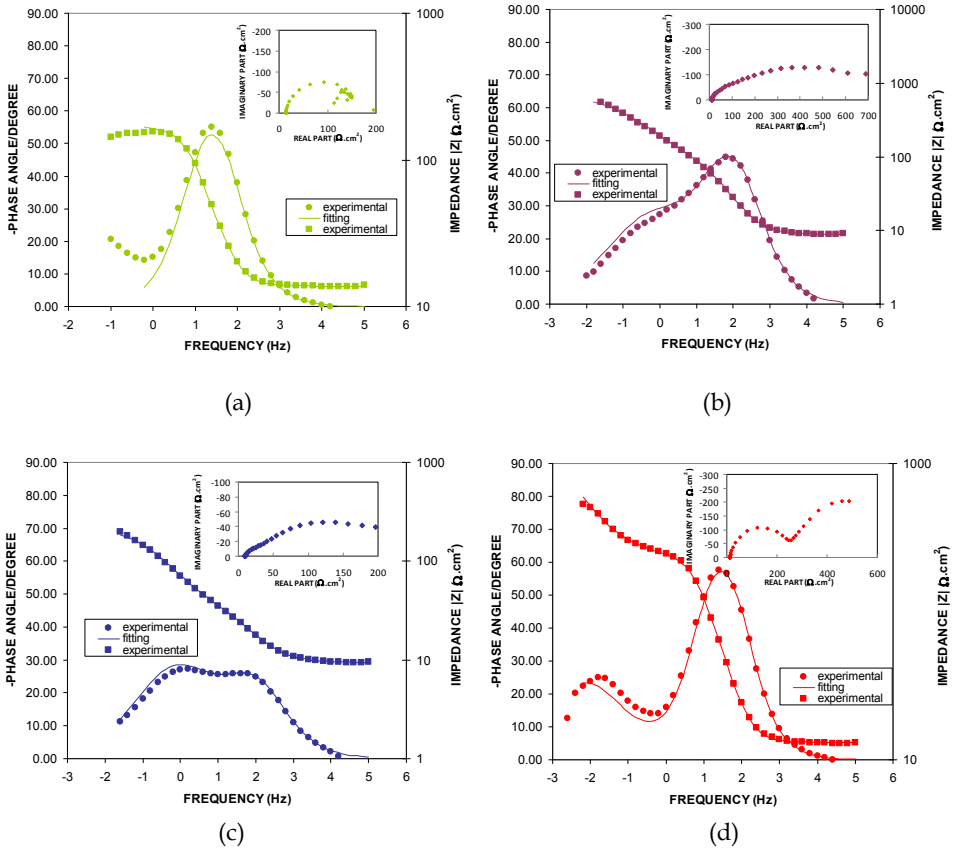


Fig. 7. Bode y Nyquist plot for – (a) ZA50-8%SiC (b) ZA27 L(CET) (c) ZA27 L(Columnar) (d) ZA27-15%SiC

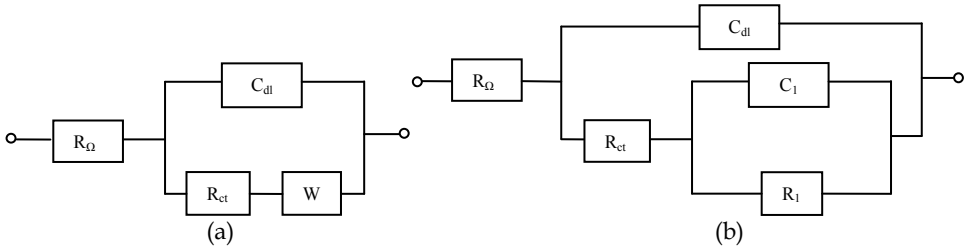


Fig. 8. Equivalent circuit of EIS for different samples.

The corrosion current can be related to the $R_{ct}$ in the case of mixed control (Epelboin et al., 1972), where the polarization resistance technique fails, according to the following expression:

$$R_{ct} = b_a\, b_c / 2.303(b_a+b_c) I_{corr} \tag{3}$$

However, it is important to note that the Rct values are not directly related to the susceptibility to corrosion of the different alloys and composites. They are related to the rate of charge transfer reactions that give rise to the formation of a passive layer on the surface of the samples (the impedance measurements are at open circuit potential only). The protective characteristics of these passive films depend on the preparation conditions of the alloys, the distribution of elements in the alloy and the presence on the surface of active sites for adsorption of chloride ion.

Ions are formed during the anodic dissolution of alloy

$$Zn \rightarrow Zn^{+2} + 2\, e^-$$

which can react with hydroxyl ions

$$H_2O + \tfrac{1}{2}\, O_2 + 2\, e^- \rightarrow 2\, OH^-$$

and can be generated $Zn(OH)_2$

The ZA27 alloy with different structures is less resistant to corrosion and its susceptibility to corrosion is dependent of the structure. The ZA27 – 15%CSi composite has the highest corrosion resistance. Also, discriminating by type of composite materials, the MMCs with SiC are more corrosion resistant than those MMCs prepared with alumina particles.

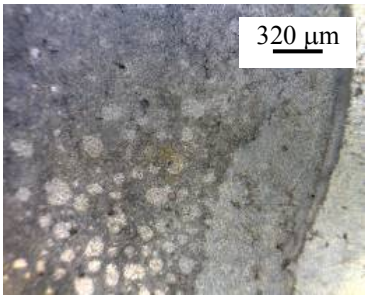


Fig. 9. Micrograph of ZA27 – 8%SiC sample after EIS test.

| Alloy / Composite (wt pct) | $R_\Omega$ ($\Omega.cm^2$) | $C_{dl}$ ($F/cm^2$) | $R_{ct}$ ($\Omega.cm^2$) | $R_1$ ($\Omega.cm^2$) | $C_1$ ($F/cm^2$) |
|---|---|---|---|---|---|
| Zn27-15%SiC | 13.03 | $7.95e^{-5}$ | 1317.23 | 278.67 | $1.35e^{-03}$ |
| Zn50-15%SiC | 16.48 | $3.65e^{-5}$ | ------ | 19.33 | $5.18e^{-05}$ |
| Zn-27Al (L-Columnar) | 8.85 | $4.85e^{-5}$ | 94.78 | 615.29 | $7.51e^{-05}$ |
| Zn-27%Al (L-CET) | 9.41 | $1.04e^{-4}$ | 26.88 | 193.42 | $6.51e^{-04}$ |
| Zn-27%Al (L-Equiaxed) | 8.56 | $5.75e^{-5}$ | 87.01 | 304.59 | $6.05e^{-04}$ |
| Zn-27%Al – 8%CSi | 14.47 | $9.22e^{-5}$ | 228.77 | | |
| Zn-27%Al – 15%$Al_2O_3$ | 12.60 | $6.94e^{-5}$ | 151.78 | | |
| Zn-27%Al – 8%$Al_2O_3$ | 11.64 | 4.22 $e^{-5}$ | 139.57 | | |

Table 3. Principal parameters obtained from the EIS analysis.

## 4. Conclusions

The highest corrosion resistance or susceptibility to corrosion is a complex function of the alloys and composite composition, structure and the exposed surface, all of which determine the protective characteristics of the film that formed on the alloys.

Alloys with a higher aluminum content have a higher corrosion resistance, mainly due to the formation of a protective film.

Even at a higher Al concentration, the corrosion resistance depends on the structure of the alloys.

The results also indicate that the corrosion resistance of Zn-Al-SiC and Zn-Al-$Al_2O_3$ MMCs composites has demonstrated the improvement in comparison to ZA alloys in 3wt% NaCl solutions.

## 5. Acknowledgment

The authors would like to thank Consejo Nacional de Investigaciones Científicas y Técnicas (CONICET) for the financial support.

## 6. References

Ares, A.E.; Schvezov, C.E. (2000) Solidification Parameters During the Columnar-to-Equiaxed Transition in Lead-Tin Alloys. *Metallurgical and Materials Transactions A*, Vol. 31, 1611-1625, ISSN 1073-5623/83

Ares, A.E.; Gueijman, S.F.; Schvezov, C.E. (2010) Experimental Study of the Columnar-to-Equiaxed Transition During Directional Solidification of Zinc-Aluminum Alloys and Composites, *J. Crystal Growth*, Vol. 312, pp. 2154-2170, ISSN 0022-0248

Ares, A.E.; Caram, R.; Schvezov, C.E. (2003) Columnar-to-Equiaxed Transition Studies in Aluminum-Magnesium and Aluminum-Zinc Alloys, *Proceedings of Light Metals 2003*, ISBN, San Diego, California, United States, March of 2003

Ares, A.E.; Gueijman, S.F.; Caram, R.; C.E. Schvezov (2005) Analysis of Solidification Parameters During Solidification of Lead and Aluminum Base Alloys. *J. Crystal Growth*, Vol. 275, pp. 235-240, ISSN 0022-0248

Ares, A.E. ; Schvezov, C.E. (2007) Influence of Solidification Thermal Parameters on the Columnar to Equiaxed Transition of Al-Zn and Zn-Al Alloys. *Metallurgical and Materials Transactions A*, Vol. 38, pp. 1485-1499, ISSN 1073-5623/83

Ares, A.E.; Gueijman, S.F.; Schvezov, C.E. (2002) Semi-Empirical Modeling for Columnar and Equiaxed Growth of Alloys. *J. Crystal Growth*, Vol. 241, pp. 235-240, ISSN 0022-0248

Ares, A.E.; Gassa, L.M.; Gueijman, S.F.; Schvezov, C.E. (2008) Correlation Between Thermal Parameters, Structures, Dendritic Spacing and Corrosion Behavior of Zn-Al Alloys With Columnar to Equiaxed Transition. *J. Crystal Growth*, Vol. 310, pp. 1355-1361, ISSN 0022-0248

Ares, A.E.; Caram, R.; Schvezov, C.E. (2006) Relation between As-Cast Mechanical Properties, Microstructure and Solidification Conditions for Zn-Al Alloys, Proceedings of MCWASP International Conference Modeling of Casting, Welding and Advance Solidification Processes – XI, Opio, France, June of 2006

Ares, A.E.; Gatti, I. P.; Gueijman, S.F.; Schvezov, C.E. (2009) Mechanical Properties of Zinc-Aluminum Alloys versus Structural and Thermal Parameters, Proceedings of MCWASP International Conference Modeling of Casting, Welding and Advance Solidification Processes – XII, Vancouver, Canadá, June of 2009

Augustynski, J. (1978) Etude De La Rupture De Passivite De Certains Metaux Electrochimiquement Actifs, *Corrosion Sci.*, Vol. 13, pp. 955-965, ISSN 0010-938X

Bilmes, P.D., Llorente, C.L., Saire Huamán, L., Gassa, L.M., Gervasi, C.A. (2005) Microstructure and pitting corrosion of 13CrNiMo weld metals. *Corrosion Science*, Vol. 48, p.p. 3261–3270, ISSN 0010-938X

Cockcroft, S. L.; Rappaz, M.; Mitchell, A. (1994) An Examination of Some of the Manufacturing Problems of Large Single-Crystal Turbine Blades for Use in Land-Based Gas Turbines, In: *Materials for Advanced Power Engineering*, Coutsouradis, J. et al., pp. 1161-1175, ISBN 0-7923-3075-7, New York: Kluwer Inc.

Deslouis, C.; Duprat, M.; Tulet-Tournillon, C. (1984) The Cathodic Mass Transport Process During Zinc Corrosion in Neutral Aerated Sodium Sulphate Solutions. *J. Electroanal Chem.*, Vol. 181, pp. 119-136, ISSN 0022-0728

Epelboin, I.; Keddam, M.; Takenouti, H. (1972) Use of Impedance Measurements for the Determination of the Instant Rate of Metal Corrosion. *Journal of Applied Electrochemistry*, Vol. 2, pp. 71-79, ISSN 0021-891X

Frankel, G.S. (1998) Pitting Corrosion of Metals. *Journal of the Electrochemical Society*, Vol. 145, pp. 2186–2198, ISSN 1945-7111

Fedrizzi, L.; Ciaghi, L.; Bonora, P.L.; Fratesi, R.; Roventi, G. (1992) Corrosion Behaviour of Electrogalvanized Steel in Sodium Chloride and Ammonium Sulphate Solutions, a Study by E.I.S. *J. Appl. Electrochem*, Vol. 22, pp. 247-254, ISSN 0021-891X

Gäumann, M.; Trivedi, R.; Kurz, W. (1997) Nucleation Ahead of the Advancing Interface in Directional Solidification, *Mater. Sci. Eng.* A, Vol. 226-228, pp. 763-769, ISSN 0921-5093, ISSN 0921-5093

Gäumann, M.; Bezençon, C.; Canalis, P. et al. (2001) Single-Crystal Laser Deposition of Superalloys: Processing-Microstructure Maps. *Acta Mater.*, Vol. 49, pp.1051-1062, ISSN 1359-6454

Hunt, J. D. (1984) Steady State Columnar and Equiaxed Growth of Dendrites and Eutectic. *Mater. Sci. Eng.*, Vol. 65, pp. 75-83, ISSN 0921-5093

Kurz, W.; Giovanola, B.; Trivedi, R. (1986) Theory of Microstructural Development During Rapid Solidification. *Acta Metall. Mater.*, Vol. 34, pp. 823-830, ISSN 0956-7151

Lipton, J.; Kurz,W.; Trivedi, R. (1987) Rapid Dendrite Growth in Undercooled Alloys. *Acta Metall.*, Vol. 35, pp.957-964, ISSN 0956-7151

Long, T.T.; Nishimura, T.; Aisaka, T.; Morita, M. (1991) Wear Resistance of Al-Si Alloys and Aluminum Matrix Composites. *Materials Transactions JIM*, Vol. 32, Nº 2, pp. 181-188, ISSN 0916-1821

McFadden S.; Browne D.J.; Gandin C.A. (2009) A Comparison of Columnar-to-Equiaxed Transition Prediction Methods Using Simulation of the Growing Columnar Front. *Metall Mater Trans A*, Vol. 40, pp. 662-672, 1073-5623

Reinhart G.; Mangelinck-Noël N.; Nguyen-Thi H.; Schenk T.; Gastaldi J.; Billia B.; Pino P.; Härtwig J.;Baruchel J. (2005) Investigation of Columnar–Equiaxed Transition and Equiaxed Growth of Aluminium Based Alloys by X-ray Radiography. *Mater Sci Eng A*, Vol. 413–414, pp. 384–388, ISSN 0921-5093

Rohatgi, P. (1991) Cast Aluminum-Matrix Composites for Automotive Applications. JOM, Vol. 43, pp. 10–15, ISSN 1047-4838

Spittle J.A. (2006) Columnar to Equiaxed Grain Transition in as Solidified Alloys. *International Materials Reviews,* Vol.51, No.4, pp. 247–269, ISSN 0950-6608

Trabanelli, G.; Zucchi, F.; Brunoro, G.; Gilli, G. (1975) Characterization of the Corrosion or Anodic Oxidation Products on Zinc. *Electrodeposition Surf. Treat.*, Vol. 3, pp. 129-138, ISSN 0300-9416

Vander Voort, G.F. (June 2007) *Metallography Principles and Practice* (Fourth Edition) , ASM International, ISBN-10: 0-87170-672-5, New York, United States

Wilde, B.E. (1972) Critical Appraisal of some Popular Laboratory Electrochemical Tests for Predicting the Localized Corrosion Resistance of Stainless Alloys in Sea Water. *Corrosion*, Vol. 28, pp. 283–291, ISSN 00109312

Zhang, X. G. (1996) *Corrosion and Electrochemistry of Zinc* (First Edition), Plenum Press, ISBN 0-306-45334-7, New York and London